ON THE DYNAMICS OF THE WEAK FRÉEDERICKSZ TRANSITION FOR NEMATIC LIQUID CRYSTALS

P. AURSAND, G. NAPOLI, AND J. RIDDER

Abstract. We consider the dynamics of the director in a nematic liquid crystal cell with an applied electric field. The bend-splay geometry is assumed, and the director is weakly anchored at the boundary. For this setting, excited equilibrium states of odd parity have been observed experimentally by Kumar et al. (2010) and investigated analytically by Bevilacqua and Napoli (2012), but the dynamics of the transition between them has so far not been the subject of much study.

An implicit finite difference method is derived for studying the time-evolution of the director field under varying voltages and anchoring strengths. The scheme solves the general nonlinear equations, i.e., it does not assert the one-constant approximation, and allows coupling with Gauss' law for the electric field. Through numerical simulation of basic transition experiments, we show how excited states of odd parity can manifest, also in the general nonlinear case.

1. Introduction

1.1. **Background.** Nematic liquid crystals usually consist of rod-shaped organic molecules for which it is energetically favorable for neighboring molecules to align. This causes macroscopic correlation in the orientation of their long axis, while the molecules themselves are free to flow like a liquid. Nematic liquid crystals have seen widespread use in display devices, due to the optical birefringence associated with the anisotropy of the molecules. Since the orientation of the long axis can be manipulated by applied electromagnetic fields, polarized light can be either stopped by or let through a liquid crystal cell, depending on the applied voltage difference.

Under the assumption of constant degree of orientation, the state of a nematic liquid crystal is often represented in terms of two linearly independent vector fields: the velocity field giving the flow and the director field giving the local average molecular orientation. In this work we will assume a steady flow field and focus on the dynamics of the director. This implies disregarding phenomena such a back-flow, which can be important in the rheology of liquid crystals [5]. Furthermore, we will restrict our discussion to a one-dimensional liquid crystal cell on $x \in [0, L]$ in the bend-splay geometry. Specifically, we assume the director $\mathbf{n}$ is fixed to the $x - y$ plane, i.e.,

$$\mathbf{n}(x,t) = (\cos(\psi(x,t)), \sin(\psi(x,t)), 0), \tag{1}$$

where ψ is the angle between the x-axis and the director. Herein, we will consider numerical solutions to the initial-value problem

$$q\psi_T - \tilde{c}(\psi)(\tilde{c}(\psi)\psi_X)_X + \frac{1}{2}h^2 \sin(2\psi)\tilde{E}^2 = 0, \qquad (X,T) \in (0,1) \times \mathbb{R}^+, \tag{2a}$$

$$\psi(X,0) = \psi_0(X), \qquad X \in (0,1), \tag{2b}$$

Date: June 18, 2015.

Key words and phrases. Nematic liquid crystals; Fréedericksz transition; Weak anchoring.

with boundary conditions

$$\psi_X + \frac{1}{2}\frac{\beta}{\tilde{c}^2(\psi)}\sin(2\psi) = 0, \quad X = 0, \tag{3a}$$

$$\psi_X - \frac{1}{2}\frac{\beta}{\tilde{c}^2(\psi)}\sin(2\psi) = 0, \quad X = 1. \tag{3b}$$

In the above, the dimensionless constants q, h and β represent dissipation, field strength and anchoring strength, respectively, and

$$\tilde{c}(\psi) = \sqrt{\cos^2(\psi) + \frac{\alpha_2}{\alpha_1}\sin^2(\psi)}.$$

The classical example of interaction between the director field and an external electric or magnetic field is the Fréedericksz transition. In its most basic form, it can be described as a competition between elastic torques resisting distortions in the director field, and electromagnetic torques aligning molecules along a preferred direction: Consider e.g. a liquid crystal cell where the the easy direction at the surfaces is fixed at $\psi = \pi/2$. The equilibrium configuration is then a homogeneous director field. An electric field is applied twisting the director towards the angle π. When the applied field is below some critical value, $E < E_{\mathrm{F}}$, elastic forces dominate and the constant director state $\psi = \pi/2$ is stable. However, when the field is sufficiently strong, $E > E_{\mathrm{F}}$, the equilibrium state becomes a nontrivial configuration where $\pi/2 < \psi \leq \pi$ in the interior of the domain. This sudden realignment is what is often referred to as the Fréedericksz transition.

Usually, the surfaces of liquid crystals are designed in such a way that the director remains strongly anchored at normal operating voltages in display devices [3]. However, it has been theorized that having more weakly anchored director fields at the surfaces could allow for lower operating voltages and quicker response times [10]. In the modeling, this can be introduced by applying *weak* boundary conditions, i.e., introducing an energy penalty for deviations from the anchoring angle [11]. As shown in Figure 1, in the weak Fréedericksz transition there are *two* critical points. The first one, as in the classic case, represents electric forces overcoming the elastic. The second, the *saturation* threshold, is reached when the electric torque is strong enough to overcome the boundary anchoring. Here, the stable configuration is a constant homeotropic ($\psi = \pi$) state.

Since it was proposed by Rapini and Papoular [11], the weak Fréedericksz transition has been an important part of the liquid crystal literature [5, 13, 12]. In their recent paper, Costa et al. [4] were able to prove a uniqueness property for stationary solutions of the weak Fréedericksz transition. Specifically, they showed that for any given values of the applied field, field susceptibility, elastic constants and anchoring energy, there exists a unique solution $\psi(x) \in [0, \pi/2]$ of the equations describing the force balance of the director field.

However, in their recent work, Kumar et al. [7] observed experimentally director states that break the even symmetry around the center of the cell. This discovery led Bevilacqua and Napoli [2] to investigate the uniqueness of minimizers of the free energy on the full interval $\psi \in [0, \pi]$. Specifically, they studied the model

$$\psi_{XX} - \frac{1}{2}h^2\sin(2\psi) = 0, \qquad X \in (0,1), \tag{4}$$

with boundary conditions

$$\psi_X + \frac{1}{2}\beta\sin(2\psi) = 0, \quad X = 0, \tag{5a}$$

$$\psi_X - \frac{1}{2}\beta\sin(2\psi) = 0, \quad X = 1, \tag{5b}$$

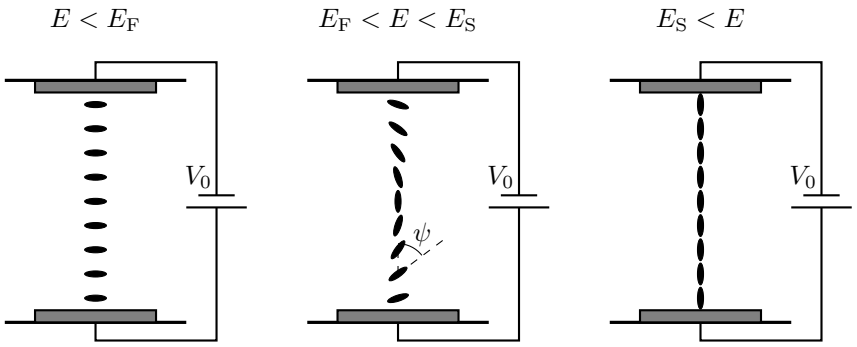

FIGURE 1. Illustration of the weak Fréedericksz transition. Left: For a low electric field the anchoring forces dominate and the director field is in a homogeneous ($\psi = \pi/2$) configuration. Middle: For electric fields above the Fréedericksz threshold but below the saturation threshold there is a competition between electric and anchoring forces leading to a nontrivial configuration. Right: For strong electric fields (over the saturation threshold) the electric forces overcome the anchoring and the configuration is homeotropic ($\psi = 0$).

where h is the dimensionless field and β is the dimensionless anchoring strength. By using direct methods and calculating exact solutions, they showed that there exists a hierarchy of excited states satisfying the stationary equations (4)–(5). Moreover, these solutions were shown to be of different parities.

The nonuniqueness of stationary solutions for the weak Fréedericksz transition makes the dynamics of the problem particularly interesting, and herein lies the main purpose of this paper. Given a constant electric field ($\tilde{E} = 1$) and the one-constant approximation ($\alpha_1 = \alpha_2$), the model (2)–(3) reduces to that of Bevilacqua and Napoli (4)–(5). However, it is not clear how the existence of excited stationary director states will effect the dynamics of the Fréedericksz transition. We aim to derive a robust and efficient numerical scheme for (2)–(3), and use this to study the evolution of the director field. Specifically, we wish to address two questions:

(1) How will excited equilibrium states manifest in the basic Fréedericksz transition experiment?
(2) Will relaxing the one-constant approximation and coupling with a nonconstant electric field influence the experiment?

To the best of our knowledge, this work is the first attempt to numerically study the dynamic transition to excited director states in the Fréedericksz transition with weak anchoring.

This paper is organized as follows: In Section 2 we use an energy variational approach to derive the basic nondimensional model under consideration (2)–(3). Different simplifications with regard to the electric field and elasticity will be also be discussed. Section 3 concerns an implicit numerical time-stepping scheme for solving the governing equations. Herein, we show the well-posedness of the nonlinear implicit equations of the discrete problem. In Section 4 we perform numerical experiments addressing the questions posed above. In particular, we will show that excited director states can be observed in numerical experiments.

2. Variational derivation of the dynamic model

The governing equations for the director field will be derived by assering an energy law for the system. The time evolution of the director field is then given by a dissipative variational principle.

2.1. **The full model.** Under the assumption that $\mathbf{n}$ is given by (1), the governing equations for the director field will be derived using the different contributions to the energy with an action principle. Expressed in terms of ψ, the bulk kinetic energy can be written as

$$W_{\mathrm{K}} = \frac{1}{2}\int_0^L \sigma\psi_t^2 \,\mathrm{d}x,$$

where σ is an inertial constant. A typical value for σ is $\sim 10^{-13}\,\mathrm{kg\,m^{-1}}$ (for the nematic MBBA [6]).

The elasticity of the liquid crystal will resist distortions in the director field. The standard model for the elasticity in nematics is given by the Oseen–Frank free energy density

$$\mathcal{W}_{OF}(\mathbf{n},\nabla\mathbf{n}) = \frac{1}{2}\alpha_1|\mathbf{n}\times(\nabla\times\mathbf{n})|^2 + \frac{1}{2}\alpha_2(\nabla\cdot\mathbf{n})^2 + \frac{1}{2}\alpha_3(\mathbf{n}\cdot(\nabla\times\mathbf{n}))^2\,. \tag{6}$$

The energy (6) is the most general form which is both quadratic in $\nabla\mathbf{n}$ and invariant with respect to the transformation $\mathbf{n}\to-\mathbf{n}$. The constants α_1, α_2 and α_3 represents bend, splay and twist distortions, respectively. For the typical liquid crystal 5CB, values have been measured to $\alpha_1 = 8.2\times10^{-12}\,\mathrm{N}$, $\alpha_2 = 6.2\times10^{-12}\,\mathrm{N}$, and $\alpha_3 = 3.9\times10^{-12}\,\mathrm{N}$. Given the director field (1), the elastic bulk energy takes the form

$$W_{\mathrm{OF}} = \frac{1}{2}\int_0^L c^2(\psi)\psi_x^2 \,\mathrm{d}x$$

with

$$c(\psi) = \sqrt{\alpha_1\cos^2(\psi) + \alpha_2\sin^2(\psi)}\,.$$

The anisotropic nature of the molecules will cause the electric displacement in the liquid crystal to depend on the director field. In what follows, we will assume that the contribution to the displacement is purely dielectric and given by

$$\mathbf{D} = \varepsilon_0(\varepsilon_\perp\mathbf{E} + \varepsilon_a(\mathbf{n}\cdot\mathbf{E})\mathbf{n})\,, \tag{7}$$

where $\varepsilon_0 = 8.854\times10^{-12}\,\mathrm{F\,m^{-1}}$ is the permittivity in free space, $\varepsilon_\perp$ is the relative permittivity perpendicular to the director ($\varepsilon_\perp = 7$ for 5CB [12]) and ε_a is the dielectric anisotropy ($\varepsilon_a = 11.5$ for 5CB [12]). The contribution to the bulk energy from the electric field is then

$$W_{\mathrm{E}} = -\frac{1}{2}\int_0^L \mathbf{E}\cdot\mathbf{D}\,\mathrm{d}x = -\frac{1}{2}\int_0^L d(\psi)E^2\,\mathrm{d}x, \tag{8}$$

where

$$d(\psi) = \varepsilon_0(\varepsilon_\perp + \varepsilon_a\cos^2(\psi)).$$

We assume that the surfaces at each end of the cell has been treated in such a way that a particular director orientation is energetically preferred. To achieve this, we apply an anchoring potential, and let

$$W_{\mathrm{B}} = \frac{1}{2}w\cos^2(\psi), \quad x = 0, L \tag{9}$$

for some constant w representing the anchoring strength. We note that for this choice the parallel (homogeneous) alignment will be energetically preferred at the boundary for $w > 0$ and, conversely, the homeotropic for $w < 0$.

The energy dissipation rate is assumed to be of the form

$$D = \frac{1}{2}\kappa \int_0^L \psi_t^2 \,\mathrm{d}x, \tag{10}$$

where κ is a dissipation constant. For the liquid crystal MBBA, $\kappa = 0.0777\,\mathrm{Pa\,s}$, [12].

Taking into account elastic, electric and boundary energies, the total energy balance takes the form

$$\begin{aligned} \frac{\mathrm{d}}{\mathrm{d}t}\Big(\frac{1}{2}\int_0^L \big(\sigma\psi_t^2 + c^2(\psi)\psi_x^2 - d(\psi)E^2\big)\mathrm{d}x + \frac{1}{2}w\cos^2(\psi)\,(|_{x=0}+|_{x=L})\Big) \\ = -\frac{1}{2}\kappa\int_0^L \psi_t^2 \,\mathrm{d}x. \end{aligned} \tag{11}$$

Following the approach from [1], we can use the dissipative principle of least action to derive the evolution equation

$$\sigma\psi_{tt} + \kappa\psi_t - c(\psi)(c(\psi)\psi_x)_x - \frac{1}{2}d'(\psi)E^2 = 0, \qquad (x,t) \in (0,L)\times\mathbb{R}^+, \tag{12}$$

with boundary conditions

$$c^2(\psi)\psi_x + \frac{w}{2}\sin(2\psi) = 0, \quad x = 0, \tag{13a}$$

$$c^2(\psi)\psi_x - \frac{w}{2}\sin(2\psi) = 0, \quad x = L. \tag{13b}$$

In the rest of this paper, we will follow common practice and assume that the inertial term can be neglected in favor of dissipative forces, i.e. $\sigma = 0$.

In general, the electric field will depend on the director configuration through Gauss' law. Under the assumptions above, we can write the field $E = -U_x$, and the equation to be solved is

$$(d(\psi)U_x)_x = 0\,,$$

with boundary conditions $U(0) = 0$ and $U(L) = V_0$. Hence, for a given director configuration, U_x can be determined by

$$U_x(x) = \frac{1}{d(\psi(x))}\Big(\int_0^L \frac{1}{d(\psi(x'))}\,\mathrm{d}x'\Big)^{-1} V_0\,. \tag{14}$$

In the interest of deriving a dimensionless version of the model (12)–(13), we introduce the scalings $X = x/L$, $T = t/\tau$ and $u = U/V_0$. Here, τ is some characteristic time scale for the dynamics of the system. Furthermore, we follow Bevilacqua and Napoli [2] and introduce the *extrapolation length*

$$\ell = \frac{\alpha_1}{w}$$

and the *electric coherence length*

$$\xi = \frac{L}{V_0}\sqrt{\frac{\alpha_1}{\varepsilon_0\varepsilon_a}}$$

Moreover, we define the nondimensional quantities

$$\tilde{c}(\psi) = \sqrt{\cos^2(\psi) + \frac{\alpha_2}{\alpha_1}\sin^2(\psi)}, \qquad h = \frac{L}{\xi}, \qquad \beta = \frac{L}{\ell} \qquad \text{and} \qquad q = \frac{L^2\kappa}{\alpha_1\tau}.$$

Using the numbers defined above, we can write (12) in the equivalent form

$$q\psi_T - \tilde{c}(\psi)(\tilde{c}(\psi)\psi_X)_X + \frac{1}{2}h^2\sin(2\psi)u_X^2 = 0, \qquad (X,T) \in (0,1)\times\mathbb{R}^+, \tag{15}$$

and for the boundary conditions (13),

$$\psi_X + \frac{1}{2}\frac{\beta}{\tilde{c}^2(\psi)}\sin(2\psi) = 0, \quad X = 0, \tag{16a}$$

$$\psi_X - \frac{1}{2}\frac{\beta}{\tilde{c}^2(\psi)}\sin(2\psi) = 0, \quad X = 1. \tag{16b}$$

2.2. **Constant electric field approximation.** The assumption that the electric field remains constant, i.e., is unaffected by the state of the director field, can be introduced by removing the coupling with Gauss' law. The nondimensional electric field is then given by $u_X = 1$, and we can replace (15) with

$$q\psi_T - \tilde{c}(\psi)(\tilde{c}(\psi)\psi_X)_X + \frac{1}{2}h^2\sin(2\psi) = 0, \qquad (X,T) \in (0,1)\times\mathbb{R}^+, \tag{17}$$

endowed with the boundary condition (16).

2.3. **One-constant approximation.** A common simplification made in the literature is the so-called one-constant approximation $\alpha_1 = \alpha_2 = \alpha_3$. Under this assumption we have $\tilde{c}(\psi) = 1$, and the nondimensional problem can be written as

$$q\psi_T - \psi_{XX} + \frac{1}{2}h^2\sin(2\psi) = 0, \qquad (X,T) \in (0,1)\times\mathbb{R}^+, \tag{18}$$

with boundary conditions

$$\psi_X + \frac{1}{2}\beta\sin(2\psi) = 0, \quad X = 0, \tag{19a}$$

$$\psi_X - \frac{1}{2}\beta\sin(2\psi) = 0, \quad X = 1. \tag{19b}$$

Remark 2.1. *A simple transformation $X \to X - 1/2$ and $\psi \to \pi/2 - \psi$ reveals that the stationary version of (18)–(19) is equivalent to the problem studied by Bevilacqua and Napoli [2].*

3. The numerical method

To define the numerical scheme, divide the interval $[0,1]$ into N cells of length ΔX and choose a time step ΔT. This gives grid points

$$(X_i, T^n) = (i\Delta X, n\Delta T),$$

where $i = 0,\dots,N$ and $n \in \mathbb{N}$. The numerical method defined below will calculate values ψ_i^n that approximate the exact solution ψ on these grid points.

The discretization defined below is based on central differences. However, derivatives in space must be handled with care to accommodate the fact that the director describes the orientation of symmetric molecules, i.e., $\mathbf{n} = -\mathbf{n}$. For example, $\psi_0^n = 0$ and $\psi_1^n = \frac{\pi}{2}$ describe physically the same situation as $\psi_0^n = 0$ and $\psi_1^n = \frac{3\pi}{2}$, and should thus give rise to the same elastic energy. Hence, the straightforward discretization $D_X\psi^n_{i+\frac{1}{2}} = \frac{1}{\Delta X}(\psi^n_{i+1} - \psi^n_i)$ is adjusted to

$$\begin{aligned} &D_X\psi^n_{i+\frac{1}{2}}\cdot\Delta X \\ &= p_{[-\frac{\pi}{2},\frac{\pi}{2})}(\psi^n_{i+1} - \psi^n_i) \\ &:= \begin{cases} (\psi^n_{i+1} - \psi^n_i) \bmod \pi & \text{if } ((\psi^n_{i+1} - \psi^n_i) \bmod \pi) \in [0, \frac{\pi}{2}), \\ ((\psi^n_{i+1} - \psi^n_i) \bmod \pi) - \pi & \text{otherwise,} \end{cases} \end{aligned}$$

which guarantees $D_X\psi^n_{i+\frac{1}{2}}\cdot\Delta X \in [-\frac{\pi}{2},\frac{\pi}{2})$. For the discretization in time such an adjustment is not necessary, because $|\psi_i^{n+1} - \psi_i^n| < \pi/2$ for sufficiently small time steps.

For better readability, define the averages

$$\psi_i^{n+\frac{1}{2}} = \frac{1}{2}(\psi_i^n + \psi_i^{n+1})\,, \qquad \sin(2\psi_i)^{n+\frac{1}{2}} = \frac{1}{2}\left(\sin(2\psi_i^n) + \sin(2\psi_i^{n+1})\right)\,,$$
$$c_i^{n+\frac{1}{2}} = \frac{1}{2}\left(\tilde{c}(\psi_i^n) + \tilde{c}(\psi_i^{n+1})\right)\,, \qquad c_{i+\frac{1}{2}}^{n+\frac{1}{2}} = \frac{1}{2}\left(c_i^{n+\frac{1}{2}} + c_{i+1}^{n+\frac{1}{2}}\right)\,,$$

and the difference operators

$$D_T\psi_i^{n+\frac{1}{2}} = \frac{1}{\Delta T}(\psi_i^{n+1} - \psi_i^n)\,, \qquad D_X\psi_{i+\frac{1}{2}}^{n+\frac{1}{2}} = \frac{1}{\Delta X}p_{[-\frac{\pi}{2},\frac{\pi}{2})}(\psi_{i+1}^{n+\frac{1}{2}} - \psi_i^{n+\frac{1}{2}})\,,$$

and accordingly,

$$D_X(c\,D_X\psi)_i^{n+\frac{1}{2}} = \frac{1}{\Delta X}\left(c_{i+\frac{1}{2}}^{n+\frac{1}{2}}(D_X\psi)_{i+\frac{1}{2}}^{n+\frac{1}{2}} - c_{i-\frac{1}{2}}^{n+\frac{1}{2}}(D_X\psi)_{i-\frac{1}{2}}^{n+\frac{1}{2}}\right)\,.$$

The following implicit finite difference scheme discretizes the nonlinear model with constant electric field (17) and weak anchroing boundary conditions (16).

Definition 1 (The numerical method)**.** *Let some initial data ψ_i^0, $i = 0,\dots,N$ be given. For each time step $n = 1,2,3,\dots$, define $\psi_1^{n+1},\dots,\psi_{N-1}^{n+1}$ by*

$$qD_T\psi_i^{n+\frac{1}{2}} - c_i^{n+\frac{1}{2}}D_X(c\,D_X\psi)_i^{n+\frac{1}{2}} + \frac{1}{2}h^2\sin(2\psi_i)^{n+\frac{1}{2}} = 0\,, \tag{20}$$

and ψ_0^{n+1}, ψ_N^{n+1} by

$$D_X\psi_{\frac{1}{2}}^{n+\frac{1}{2}} + \frac{\beta}{2c_{\frac{1}{2}}^{n+\frac{1}{2}}c_0^{n+\frac{1}{2}}}\sin(2\psi_0^{n+\frac{1}{2}}) = 0\,, \tag{21a}$$

$$D_X\psi_{N-\frac{1}{2}}^{n+\frac{1}{2}} - \frac{\beta}{2c_{N-\frac{1}{2}}^{n+\frac{1}{2}}c_N^{n+\frac{1}{2}}}\sin(2\psi_N^{n+\frac{1}{2}}) = 0\,. \tag{21b}$$

A corresponding discrete version of the energy (11) is given by

$$\begin{aligned} E^n = \frac{\Delta X}{2}\left(\sum_{i=1}^{N-1}\left(c_{i+\frac{1}{2}}^n\right)^2\left(D_X\psi_{i+\frac{1}{2}}^n\right)^2 - h^2\left(\frac{\varepsilon_\perp}{\varepsilon_a} + \cos^2(\psi_i^n)\right)\right) \\ + \frac{\beta}{2}\Big(\cos^2(\psi_0^n) + \cos^2(\psi_N^n)\Big). \end{aligned} \tag{22}$$

In the following we will show that the implicit equations that define the scheme have a unique solution. Furthermore, we will prove that scheme conserves approximately a discrete energy and converges to the exact solution as ΔX and ΔT go to zero.

3.1. **Well-definedness of the scheme.** For fixed ψ_i^n, $i = 0,\dots,N$, equations (20)–(21) can be written in the fixed point form

$$(\psi_0^{n+1},\dots,\psi_N^{n+1}) = \mathcal{F}(\psi_0^{n+1},\dots,\psi_N^{n+1})\,,$$

where $\mathcal{F}$ is given by

$$(\mathcal{F}(\psi_0^{n+1},\dots,\psi_N^{n+1}))_i = \psi_i^n + \frac{\Delta T}{q}c_i^{n+\frac{1}{2}}D_X(c\,D_X\psi)_i^{n+\frac{1}{2}} - \frac{\Delta T}{2q}h^2\sin(2\psi_i)^{n+\frac{1}{2}}\,, \tag{23a}$$

for $i = 1, \dots, N-1$, and, for ΔX sufficiently small,

$$(\mathcal{F}(\psi_0^{n+1}, \dots, \psi_N^{n+1}))_0 = -\psi_0^n + 2\psi_1^{n+\frac{1}{2}} + \frac{\beta \Delta X}{c_{\frac{1}{2}}^{n+\frac{1}{2}} c_0^{n+\frac{1}{2}}} \sin(2\psi_0^{n+\frac{1}{2}}) \,, \tag{23b}$$

$$(\mathcal{F}(\psi_0^{n+1}, \dots, \psi_N^{n+1}))_N = -\psi_N^n + 2\psi_{N-1}^{n+\frac{1}{2}} + \frac{\beta \Delta X}{c_{N-\frac{1}{2}}^{n+\frac{1}{2}} c_N^{n+\frac{1}{2}}} \sin(2\psi_N^{n+\frac{1}{2}}) \,. \tag{23c}$$

Hence, (20)–(21) have a solution if $\mathcal{F}$ is a contraction.

To show this, first define the constants

$$\begin{aligned}
|\widetilde{c}(\psi)| &= \sqrt{\cos^2(\psi) + \frac{\alpha_2}{\alpha_1} \sin^2(\psi)} \leq \max\left(1, \sqrt{\frac{\alpha_2}{\alpha_1}}\right) =: C_1 \,, \\
|\widetilde{c}'(\psi)| &= \frac{|\frac{\alpha_2}{\alpha_1} - 1||\sin(\psi)\cos(\psi)|}{\sqrt{\cos^2(\psi) + \frac{\alpha_2}{\alpha_1} \sin^2(\psi)}} \leq \frac{\frac{1}{2}|\frac{\alpha_2}{\alpha_1} - 1|}{\min\left(1, \sqrt{\frac{\alpha_2}{\alpha_1}}\right)} =: C_2 \,, \\
|\widetilde{c}(\psi)| &= \sqrt{\cos^2(\psi) + \frac{\alpha_2}{\alpha_1} \sin^2(\psi)} \geq \min\left(1, \sqrt{\frac{\alpha_2}{\alpha_1}}\right) =: C_3 \,,
\end{aligned}$$

and note that if $\|\psi^n\|_{l^\infty} \leq K_0$, for some constant K_0, then

$$|\mathcal{F}(\psi^{n+1})_i| \leq K_0 + \frac{\Delta T}{q} C_1^2 \frac{1}{\Delta X^2} (2(K_0 + \|\psi^{n+1}\|_{l^\infty})) + \frac{\Delta T}{2q} h^2 \,,$$

for $i = 1, \dots, N-1$,

$$|\mathcal{F}(\psi^{n+1})_0| \leq K_0 + 2\left(\frac{1}{2}(K_0 + \mathcal{F}(\psi^{n+1})_1)\right) + \frac{\beta}{C_3^2} \Delta X \,,$$

and similarly for $|\mathcal{F}(\psi^{n+1})_N|$.

Next, choose some $K_1, K_2, K_3 > 0$ and ΔX, ΔT, such that

$$\Delta X \leq \frac{C_3^2}{\beta} K_1 \,, \tag{24a}$$

$$\Delta T \leq \frac{2q}{h^2} K_2 \,, \tag{24b}$$

$$\Delta T \leq \frac{q}{2C_1^2} \frac{K_3 \Delta X^2}{K_0 + (3K_0 + K_1 + K_2 + K_3)} \,. \tag{24c}$$

Then, for $\|\psi^{n+1}\|_{l^\infty} \leq 3K_0 + K_1 + K_2 + K_3$, we have

$$\begin{aligned}
|\mathcal{F}(\psi^{n+1})_i| &\leq K_0 + K_2 + K_3 \,, \quad \text{for } i = 1, \dots, N-1, \\
|\mathcal{F}(\psi^{n+1})_0| &\leq K_0 + 2 \cdot \frac{1}{2}(K_0 + (K_0 + K_2 + K_3)) + K_1 \\
&= 3K_0 + K_1 + K_2 + K_3 \,, \\
|\mathcal{F}(\psi^{n+1})_N| &\leq 3K_0 + K_1 + K_2 + K_3 \,,
\end{aligned}$$

i.e., $\|\mathcal{F}(\psi^{n+1})\|_{l^\infty} \leq 3K_0 + K_1 + K_2 + K_3$.

Since ψ describes the angle of the director, we can choose $K_0 = \pi$. For any $K > 3K_0$, set $K_i = K/3 - K_0$ for $i = 1, 2, 3$, and choose ΔT and ΔX according to (24). Above we have shown that $\mathcal{F}$ maps

$$B_K := \{\psi^{n+1} | \|\psi^{n+1}\|_{l^\infty} \leq K\}$$

on (a subset of) itself. The following theorem states that $\mathcal{F}$ is also a contraction on B_K, from which follows that $\mathcal{F}$ has a unique fix point in B_K and hence the implicit equations that define the scheme have a unique solution.

Theorem 1. *The function $\mathcal{F}$ defined in* (23) *is a contraction on B_K with respect to the l^∞-norm if ΔT and ΔX satisfy* (24) *and in addition,*

$$\Delta T\left(\frac{C_A}{\Delta X^2}+C_{B_1}\right)+\Delta X C_{B_2}<1$$

for C_A, C_{B_1}, C_{B_2} defined by (25) *below, depending only on K and the physical constants α_1, α_2, h, q, and β.*

Proof. In the following, we will prove that for arbitrary ψ^{n+1} and $\widehat{\psi}^{n+1}$,

$$\|\mathcal{F}(\widehat{\psi}^{n+1})-\mathcal{F}(\psi^{n+1})\|_{l^\infty}\le C\|\widehat{\psi}^{n+1}-\psi^{n+1}\|_{l^\infty}\,,$$

for some $C<1$. Note that ψ^n in the definition of $\mathcal{F}$ is the same for both $\mathcal{F}(\psi^{n+1})$ and $\mathcal{F}(\widehat{\psi}^{n+1})$. For the sake of brevity, define $\widehat{c}_i^{\,n+\frac12}=(\widetilde{c}(\psi_i^n)+\widetilde{c}(\widehat{\psi}_i^{n+1}))/2$.

For $i=1,\dots,N-1$,

$$\begin{aligned}|\mathcal{F}(\widehat{\psi}^{n+1})_i-\mathcal{F}(\psi^{n+1})_i|\le\frac{\Delta T}{q}\Big(&|\widehat{c}_i^{\,n+\frac12}-c_i^{n+\frac12}||D_X(\widehat{c}D_X\widehat{\psi})_i^{n+\frac12}|\\&+|c_i^{n+\frac12}||D_X((\widehat{c}-c)D_X\widehat{\psi})_i^{n+\frac12}|\\&+|c_i^{n+\frac12}||D_X(c(D_X(\widehat{\psi}-\psi)))_i^{n+\frac12}|\Big)\\&+\frac{h^2\Delta T}{2q}|\sin(2\psi_i)^{n+\frac12}-\sin(2\widehat{\psi}_i)^{n+\frac12}|\,.\end{aligned}$$

This can be further bounded by

$$\begin{aligned}&|\widehat{c}_i^{\,n+\frac12}-c_i^{n+\frac12}||D_X(\widehat{c}D_X\widehat{\psi})_i^{n+\frac12}|\\&\le\frac{1}{\Delta X}\|\widetilde{c}'\|_{l^\infty}\|\widetilde{c}\|_{l^\infty}|\widehat{\psi}_i^{n+1}-\psi_i^{n+1}|\|D_X\widehat{\psi}_{i+\frac12}^{n+\frac12}\|_{l^\infty}\\&\le\frac{1}{2\Delta X}C_1C_2|\widehat{\psi}_i^{n+1}-\psi_i^{n+1}|(\|D_X\widehat{\psi}_{i+\frac12}^{n+1}\|_{l^\infty}+\|D_X\psi_{i+\frac12}^{n}\|_{l^\infty})\\&\le\frac{C_1C_2}{\Delta X^2}(\|\widehat{\psi}^{n+1}\|_{l^\infty}+\|\psi^n\|_{l^\infty})\|\widehat{\psi}^{n+1}-\psi^{n+1}\|_{l^\infty}\,,\end{aligned}$$

and in the same manner

$$\begin{aligned}|c_i^{n+\frac12}||D_X((\widehat{c}-c)D_X\widehat{\psi})_i^{n+\frac12}|&\le\frac{C_1C_2}{\Delta X^2}(\|\widehat{\psi}^{n+1}\|_{l^\infty}+\|\psi^n\|_{l^\infty})\|\widehat{\psi}^{n+1}-\psi^{n+1}\|_{l^\infty}\,,\\|c_i^{n+\frac12}||D_X(c(D_X(\widehat{\psi}-\psi)))_i^{n+\frac12}|&\le\frac{2\,C_1^2}{\Delta X^2}\|\widehat{\psi}^{n+1}-\psi^{n+1}\|_{l^\infty}\,,\\|\sin(2\psi_i)^{n+\frac12}-\sin(2\widehat{\psi}_i)^{n+\frac12}|&\le\|\widehat{\psi}^{n+1}-\psi^{n+1}\|_{l^\infty}\,.\end{aligned}$$

Putting the above estimates together, we arrive at

$$\begin{aligned}&|\mathcal{F}(\psi^{n+1})_i-\mathcal{F}(\widehat{\psi}^{n+1})_i|\\&\le\left(\frac{2}{q}C_1(C_1+C_2(\|\widehat{\psi}^{n+1}\|_{l^\infty}+\|\psi^n\|_{l^\infty}))\frac{\Delta T}{\Delta X^2}+\frac{h^2}{2q}\Delta T\right)\|\widehat{\psi}^{n+1}-\psi^{n+1}\|_{l^\infty}\,,\end{aligned}$$

for $i = 1, \dots, N-1$. For $i = 0$,

$$
\begin{aligned}
|\mathcal{F}(\psi^{n+1})_0 - \mathcal{F}(\widehat{\psi}^{n+1})_0| \leq |\psi_1^{n+1} - \widehat{\psi}_1^{n+1}| \\
&+ \beta \Delta X \Bigg(\left| \frac{1}{\widehat{c}_{\frac{1}{2}}^{n+\frac{1}{2}}} - \frac{1}{c_{\frac{1}{2}}^{n+\frac{1}{2}}} \right| \frac{1}{\widehat{c}_0^{n+\frac{1}{2}}} |\sin(2\widehat{\psi}_0^{n+\frac{1}{2}})| \\
&\quad + \frac{1}{c_{\frac{1}{2}}^{n+\frac{1}{2}}} \left| \frac{1}{\widehat{c}_0^{n+\frac{1}{2}}} - \frac{1}{c_0^{n+\frac{1}{2}}} \right| |\sin(2\widehat{\psi}_0^{n+\frac{1}{2}})| \\
&\quad + \frac{1}{c_{\frac{1}{2}}^{n+\frac{1}{2}}} \frac{1}{c_0^{n+\frac{1}{2}}} \left| \sin(2\widehat{\psi}_0^{n+\frac{1}{2}}) - \sin(2\psi_0^{n+\frac{1}{2}}) \right| \Bigg).
\end{aligned}
$$

The terms on the right-hand side can be bounded by

$$
\begin{aligned}
|\psi_1^{n+1} - \widehat{\psi}_1^{n+1}| &= |\mathcal{F}(\psi^{n+1})_1 - \mathcal{F}(\widehat{\psi}^{n+1})_1| \\
&\leq \left(\frac{2}{q} C_1 (C_1 + C_2(\|\widehat{\psi}^{n+1}\|_{l^\infty} + \|\psi^n\|_{l^\infty})) \frac{\Delta T}{\Delta X^2} + \frac{h^2}{2q} \Delta T \right) \|\widehat{\psi}^{n+1} - \psi^{n+1}\|_{l^\infty},
\end{aligned}
$$

$$
\begin{aligned}
\left| \frac{1}{\widehat{c}_{\frac{1}{2}}^{n+\frac{1}{2}}} - \frac{1}{c_{\frac{1}{2}}^{n+\frac{1}{2}}} \right| \frac{1}{\widehat{c}_0^{n+\frac{1}{2}}} |\sin(2\widehat{\psi}_0^{n+\frac{1}{2}})| &= \frac{|c_{\frac{1}{2}}^{n+\frac{1}{2}} - \widehat{c}_{\frac{1}{2}}^{n+\frac{1}{2}}|}{\widehat{c}_{\frac{1}{2}}^{n+\frac{1}{2}} c_{\frac{1}{2}}^{n+\frac{1}{2}} \widehat{c}_0^{n+\frac{1}{2}}} |\sin(2\widehat{\psi}_0^{n+\frac{1}{2}})| \\
&\leq \frac{C_2}{2C_3^3} \|\widehat{\psi}^{n+1} - \psi^{n+1}\|_{l^\infty},
\end{aligned}
$$

$$
\begin{aligned}
\frac{1}{c_{\frac{1}{2}}^{n+\frac{1}{2}}} \left| \frac{1}{\widehat{c}_0^{n+\frac{1}{2}}} - \frac{1}{c_0^{n+\frac{1}{2}}} \right| |\sin(2\widehat{\psi}_0^{n+\frac{1}{2}})| &= \frac{|c_0^{n+\frac{1}{2}} - \widehat{c}_0^{n+\frac{1}{2}}|}{c_{\frac{1}{2}}^{n+\frac{1}{2}} \widehat{c}_0^{n+\frac{1}{2}} c_0^{n+\frac{1}{2}}} |\sin(2\widehat{\psi}_0^{n+\frac{1}{2}})| \\
&\leq \frac{C_2}{2C_3^3} \|\widehat{\psi}^{n+1} - \psi^{n+1}\|_{l^\infty},
\end{aligned}
$$

$$
\frac{1}{c_{\frac{1}{2}}^{n+\frac{1}{2}}} \frac{1}{c_0^{n+\frac{1}{2}}} \left| \sin(2\widehat{\psi}_0^{n+\frac{1}{2}}) - \sin(2\psi_0^{n+\frac{1}{2}}) \right| \leq \frac{2}{C_3^2} \|\widehat{\psi}^{n+1} - \psi^{n+1}\|_{l^\infty}.
$$

Hence we get the estimate

$$
\begin{aligned}
&|\mathcal{F}(\psi^{n+1})_0 - \mathcal{F}(\widehat{\psi}^{n+1})_0| \\
&\leq \left(\frac{2}{q} C_1 (C_1 + C_2(\|\widehat{\psi}^{n+1}\|_{l^\infty} + \|\psi^n\|_{l^\infty})) \frac{\Delta T}{\Delta X^2} + \frac{h^2}{2q} \Delta T \right. \\
&\qquad \left. + \left(\beta \frac{C_2}{C_3^3} + \frac{2\beta}{C_3^2} \right) \Delta X \right) \|\widehat{\psi}^{n+1} - \psi^{n+1}\|_{l^\infty}.
\end{aligned}
$$

Analogously, one can derive a bound for $i = N$. Altogether,

$$
\|\mathcal{F}(\widehat{\psi}^{n+1}) - \mathcal{F}(\psi^{n+1})\|_{l^\infty} \leq \left(C_A \frac{\Delta T}{\Delta X^2} + C_{B_1} \Delta T + C_{B_2} \Delta X \right) \|\widehat{\psi}^{n+1} - \psi^{n+1}\|_{l^\infty},
$$

where

$$C_A = \frac{2}{q} C_1 (C_1 + C_2(K+\pi)) \,, \tag{25a}$$

$$C_{B_1} = \frac{h^2}{2q} \,, \tag{25b}$$

$$C_{B_2} = \beta \frac{C_2}{C_3^3} + \frac{2\beta}{C_3^2} \,, \tag{25c}$$

and hence, for suitable ΔT and ΔX, the function $\mathcal{F}$ is a contraction. □

In practice, we solve the implicit equations (20)–(21) using a Newton-Rhapson iteration.

3.2. **Varying electric field.** The numerical method from Definition 1 can be extended to solve the full model (15)–(16). Given a numerical solution $\psi^n = (\psi_0^n, \ldots, \psi_N^n)$ for the director field, the discrete electric field is approximated as

$$(u_{X,i})^n = \frac{1}{\Delta X} \frac{1}{\tilde{d}(\psi_i^n)} \left(\sum_{j=0}^{N} \frac{1}{\tilde{d}(\psi_j^n)} \right)^{-1} , \tag{26}$$

where $\tilde{d}(\psi)$ is the nondimensional version of $d(\psi)$,

$$\tilde{d}(\psi) = 1 + \frac{\epsilon_a}{\epsilon_\perp} \cos^2(\psi) \,.$$

By defining the shorthand notation

$$(u_{X,i}^2)^{n+\frac{1}{2}} = \frac{1}{2} \left((u_{X,i}^n)^2 + (u_{X,i}^{n+1})^2 \right) , \tag{27}$$

we can propose the following numerical scheme:

Definition 2 (The numerical method with coupled electric field)**.** *Let some initial data ψ_i^0, $i = 0, \ldots, N$ be given. For each time step $n = 1, 2, 3, \ldots$, define $(u_{X,1})^n, \ldots, (u_{X,N-1})^n$ by* (26)*, $\psi_1^{n+1}, \ldots, \psi_{N-1}^{n+1}$ by*

$$q D_T \psi_i^{n+\frac{1}{2}} - c_i^{n+\frac{1}{2}} D_X (c\, D_X \psi)_i^{n+\frac{1}{2}} + \frac{1}{2} h^2 \sin(2\psi_i)^{n+\frac{1}{2}} (u_{X,i}^2)^{n+\frac{1}{2}} = 0, \tag{28}$$

and ψ_0^{n+1}, ψ_N^{n+1} by (21)*.*

Again, the time stepping can be performed by solving the $2N$ nonlinear implicit equations(26), (28), and (21) for ψ^{n+1} and u_X^n.

4. Numerical experiments

The purpose of this section is to perform numerical experiments on the dynamics of the weak Fréedericksz transition, using the numerical scheme described in Section 3. Two experiments will be considered, illustrated in Figure 2. Both involve studying the evolution of the director configuration when h and β are changed to cross the Fréedericksz threshold h_{F} and the saturation threshold h_{S}, given implicitly by

$$h_{\mathrm{F}} = \sqrt{\frac{\alpha_1}{\alpha_2}} \beta \cot \left(\sqrt{\frac{\alpha_1}{\alpha_2}} \frac{h_{\mathrm{F}}}{2} \right) \qquad \text{and} \qquad h_{\mathrm{S}} = \beta \coth \left(\frac{h_{\mathrm{S}}}{2} \right) , \tag{29}$$

respectively [9, 13].

The first experiment illustrates the classic weak Fréedericksz transition shown in Figure 1. The director state is initially homogeneous ($\psi = \pi/2$) and $h < h_{\mathrm{F}}$. The field is then increased gradually until it is above the Fréedericksz threshold, and finally above the saturation threshold.

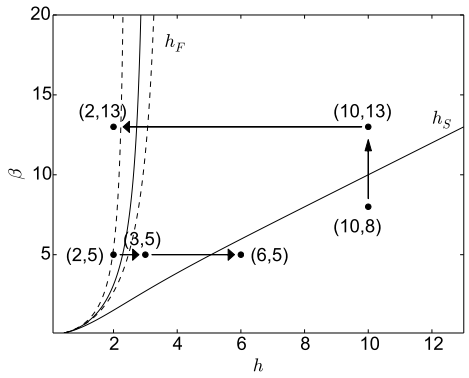

FIGURE 2. The two basic numerical experiments. Bottom: The anchoring $\beta = 5$ is kept constant while the field is increased gradually until it gets above h_{F}, and then finally until it crossed the saturation threshold h_{S}. Top: A cooling increases the anchoring to cross the saturation threshold, then a field reduction brings the state below h_{F}. Dashed lines indicate the Fréedericksz threshold h_F for $\alpha_2/\alpha_1 = 1 \pm 0.4$.

The second experiment involves a director initially in the homeotropic ($\psi = 0$) state. First, the liquid crystal is cooled, giving an increase in the anchoring strength β. Then, the field is reduced until $h < h_{\mathrm{F}}$, where the ground state is the homogeneous configuration.

A constant equilibrium state ψ is a stationary solution to (2), independently of the values of h and β. In order to facilitate the transition from a non-stable equilibrium state, we therefore add small stochastic perturbations to the homogeneous ($\psi = \pi/2$) and the homeotropic ($\psi = 0$) initial data in the numerical experiments. Specifically, we generate a zero-averaged fractional Brownian motion

$$\{S_n\}_{n=1}^{N}, \quad \sum_{n=1}^{N} S_n = 0, \quad |S_{n+1} - S_n| \leq 1, \tag{30}$$

with Hurst parameter $H = 0.9$. We then let the discrete initial data be given as

$$\psi_i^0 = \frac{\pi}{2} + \delta\, S_i + r\, \delta_S, \tag{31}$$

where $r \in [-0.5, 0.5]$ is a uniformly distributed random number and $\delta, \delta_S > 0$ are small parameters. In the following we will use $\delta = 0.01$ and $\delta_S = 0.015$.

All numerical simulations in this section are performed using $N = 100$ computational cells, if not stated otherwise. The time step is set according to

$$\Delta T = 0.3 \frac{\Delta X}{1 + \alpha_2/\alpha_1}. \tag{32}$$

The dimensionless number q is set to 1 for all experiments. For typical values of $\kappa \approx 1 \times 10^{-1}$ and $\alpha_1 \approx 1 \times 10^{-11}$, and assuming $L = 1 \times 10^{-6}\,\mathrm{m}$, this implies a characteristic time scale $\tau \approx 1 \times 10^{-2}\,\mathrm{s}$.

For the time stepping, the implicit N nonlinear equations (including the boundary conditions) are solved using a standard Newton–Raphson scheme. In each time step, the configuration from the previous step is taken as an initial guess and the iteration is performed until machine precision has been reached.

4.1. **Convergence.** The convergence behavior of the implicit scheme is investigated in the following. A numerical solution was calculated for a perturbed homogeneous ($\psi = \pi/2$) initial data with $h = 4$ and $\beta = 5$ and grid size $N = N_0 = 100$. The grid was refined according to $N_k = 2^k N_0$ with $k = 0, \cdots, 4$, generating numerical solutions $\psi^{(k)}$ at $T = 1$. The error between consecutive solutions was calculated according to

$$\mathcal{E}_k = \frac{\|\psi^{(k)} - \psi^{(k-1)}\|_{L^2(0,1)}}{\|\psi^{(k-1)}\|_{L^2(0,1)}}. \tag{33}$$

In addition to the convergence of the numerical solutions, we also verify that the energy law (11) is fulfilled in the discrete sense. Specifically, we look at the residual

$$\mathrm{Res}^{n+\frac{1}{2}} = D_T E^{n+\frac{1}{2}} - \frac{1}{2} q \Delta X \sum_{i=0}^{N} D_T \psi_i^{n+\frac{1}{2}}, \tag{34}$$

where $E^{n+\frac{1}{2}} = (E^n + E^{n+1})/2$ is the discrete energy defined in (22), and calculate $\Delta T \sum_n (\mathrm{Res}^{n+\frac{1}{2}})^2$ as the grid is refined. Figure 3 shows the convergence results, and it indicates that the numerical solutions converge to second order both in the norm and in the energy balance.

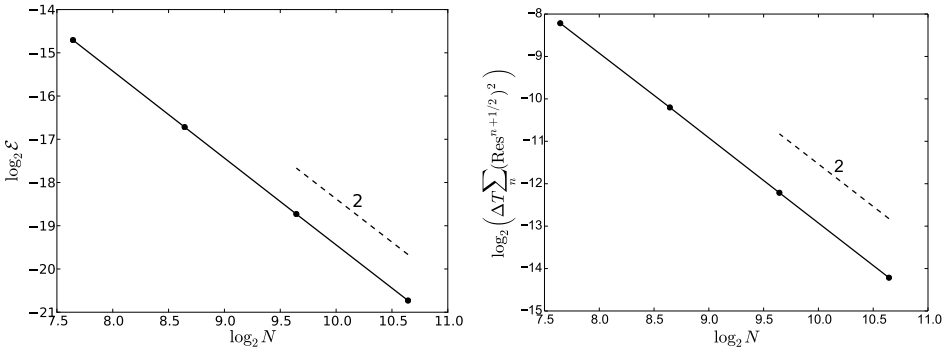

FIGURE 3. Convergence of the error under grid refinement (33) at $T = 1$ (left) and the integrated residual of the discrete energy law (34) from $T = 0$ to $T = 1$ (right). Dashed lines indicate the slope corresponding to second-order convergence.

4.2. **Weak Fréedericksz transition.** In order to verify the basic force balance of the weak Fréedericksz transtion shown in Figure 1, we perform the following numerical experiment: Initially, we set $h = 2$ and $\beta = 5$, consistent with a stable homogeneous ($\psi = \pi/2$) configuration. Also, for simplicity, we assume the one-constant approximation. At $T \in (0.5, 1)$ the field h is increased linearly to $h = 3$, which is beyond the critical thereshold h_{F}. The director field is then allowed to stabilize until $T = 3.5$, for which the field is again increased linearly until it reaches a value beyond the saturation threshold ($h = 6$). Figure 4 shows the evolution of both the director configuration and the energy. The behavior is as expected according to the classical picture of the weak Fréedericksz transition.

4.3. **Relaxing the one-constant approximation.** The basic transition experiment from Section 4.2 can also be studied numerically in the nonlinear case, i.e., by letting $\alpha_1 \neq \alpha_2$. The extrapolation length and coherence length will be defined using α_1 as before for comparison.

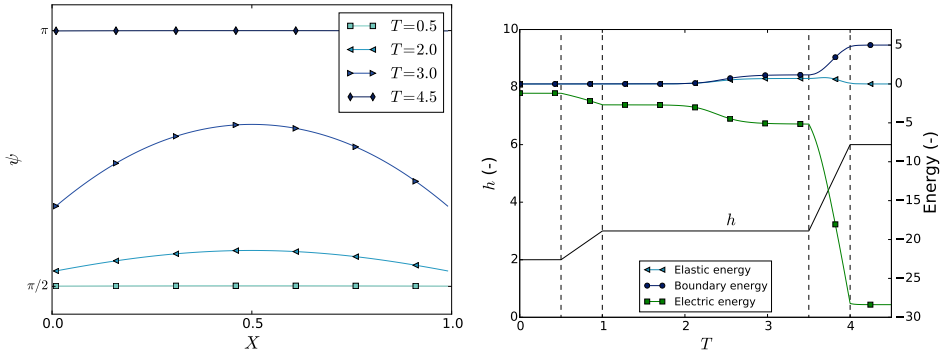

FIGURE 4. Evolution of the director field (left) and the discrete energy (22) (right) for the gradual increase of the electric field from $h = 2$ to $h = 6$. The anchoring is held constant at $\beta = 5$ and the one-constant approximation is assumed.

Figure 5 shows a snapshot of the director configuration during the Fréedericksz transition ($T = 2$) and during the saturation ($T = 3.75$). In the first case the influence of the nonlinearity is significant, even for modest perturbations from the one-constant approximation. For comparison, $\alpha_2/\alpha_1 \approx 0.75$ at room temperature for the liquid crystal 5CB [8]. Note that in general both the equilibrium configurations and the time evolution will be different when replacing the one-constant approximation with an $\alpha_2/\alpha_1 \neq 1$.

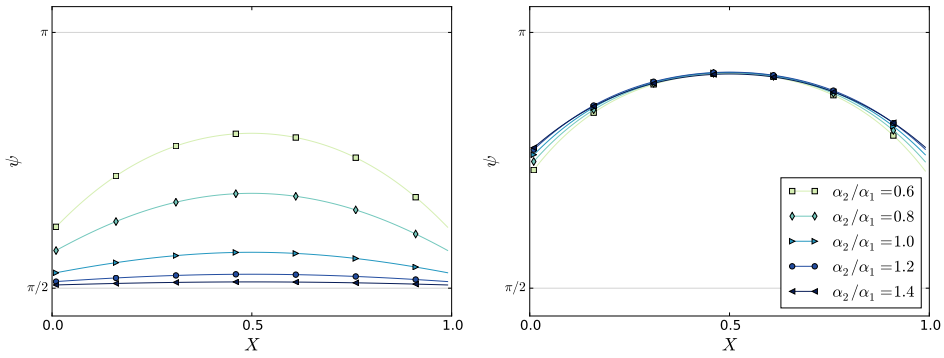

FIGURE 5. The director configuration at $T = 2$ (left) and at $T = 3.75$ (right) for the weak Fréedericksz transition experiment for different values of α_2/α_1. The electric field is assumed constant.

4.4. **Coupling with an electric field.** Using the method from Section 3.2, the weak transition experiment can also be performed with a coupled electric field. Since in this case the value of the electric field is not given a priori, the parameter h must be interpreted in a slightly weaker sense. Since it is based on the applied voltage difference V_0, h now represents represents the *average* field strength V_0/L, not the actual electric field E since this will vary both in space and in time.

Figure 6 shows the director configuration and the electric field at $T = 2$, for different values of the relative electric anisotropy $\varepsilon_a/\varepsilon_\perp$. For simplicity, the one-constant approximation ($\alpha_1 = \alpha_2$) was used. The case $\varepsilon_a/\varepsilon_\perp = 0$ represents an uncoupled electric field, and the results indicate significant differences in the

director only for large values of the electric anisotropy. As a comparison, $\varepsilon_a/\varepsilon_\perp \approx 1.64$ at room temperature for the liquid crystal 5CB [8].

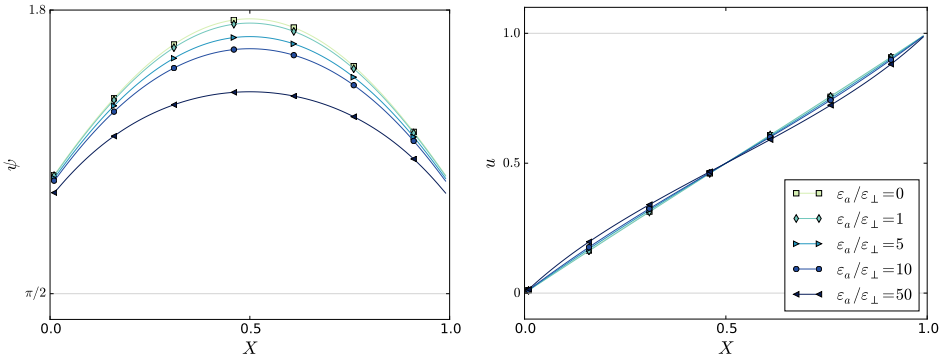

FIGURE 6. The director configuration (left) and the electric potential (right) at $T = 2$ for the weak Fréedericksz transition experiment for different values of $\varepsilon_a/\varepsilon_\perp$ using the one-constant approximation.

Explicit general solutions for the case with a fully coupled electric field are not available. However, certain approximate solutions can be found given simplifying assumptions. In particular, Napoli [9] considers the fully coupled problem with an applied electric field. Using asymptotic matching, an explicit approximate solution is calculated for large voltages V_0 and assuming the one-constant approximation.

To compare with the approximate solution, the fully coupled problem was solved using $h = 25$ and $\beta = 30$ with the one-constant approximation. Figure 7 shows the evolution of the director configuration compared with the approximation. A small, but noticable, difference can be observed between the steady-state solution and the large-voltage approximation.

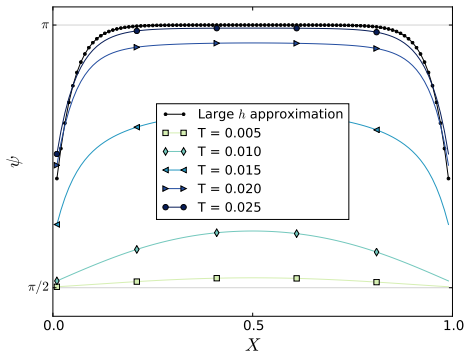

FIGURE 7. The evolution of the director configuration for the fully coupled problem using $h = 25$ and $\beta = 30$ and assuming the one-constant approximation. The initial data was a perturbed homogeneous configuration. The dotted line is the analytical approximation given by Napoli [9].

4.5. **Solutions of different parity.** In this experiment we consider a director field initially in the homeotropic state with $h = 10$ and $\beta = 8$. At $T \in [0, 0.5]$ we increase β linearly to 13, simulating a cooling of the sample. The stronger boundary anchoring will then initiate an inverse Fréedericksz transition near the ends of the sample, giving a nontrivial even or odd symmetric state, depending on the initial perturbation. At $T \in [0.8, 1.2]$ we reduce h linearly to 2, representing a gradual reduction in the electric field. Because of the reduced electric bulk energy, the new ground state will then be a homogeneous director configuration.

The results show that, depending on the initial perturbation, the final state might end up in the ground state or an excited high-energy state. Figure 8 shows that for one of the perturbations (solid lines) we first have a transition to the even symmetric ground state for $\beta = 13$ and $h = 10$ at around $T = 0.6$. When the electric field is reduced at $T = 0.8$ the director then relaxes to the homogeneous ground state. For the second random initial perturbation the cooling at $T \in [0, 0.5]$ leaves the director in an excited odd symmetric state. When the field is reduced we then obtain an excited state also for $\beta = 13, h = 2$. Figure 9 shows the different contributions to the energy, for both solutions, as a function of time.

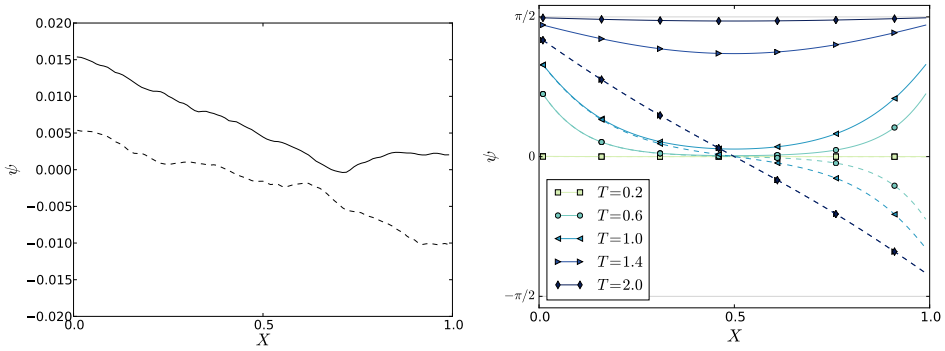

(A) Initial pertubations ($T = 0$) (B) Director evolution

FIGURE 8. The evolution of the director field for the two different initial pertubarions. The initial perturbation displayed with the solid (respectively dashed) line at the left corresponds to the evolution showed with solid (respectively dashed) lines to the right.

These results were reproduced in the nonlinear case ($\alpha_2/\alpha_1 = 0.75$) and with a coupled electric field with $\varepsilon_a/\varepsilon_\perp = 1.64$. The director evolution was almost indistinguishable from that seen in Figure 8, and is omitted here for brevity. These results indicate that odd director states also exist for models more general than the linear uncoupled case that was analyzed in [2].

5. SUMMARY

We have studied the dynamics of the director field for the classical Fréedericksz transition in the bend-splay geometry with weak anchoring. For the dimensionless problem we have derived a simple, robust and efficient numerical method. The scheme can be used both for unequal elastic constants and with a coupled electric field. We have proved that the nonlinear discrete equations are well-posed for sufficiently small time steps.

Numerical experiments have been performed for basic transition experiments where the applied electric field and the anchoring strength are varied. Herein, the transition from a ground state to an excited (odd parity) state have been observed

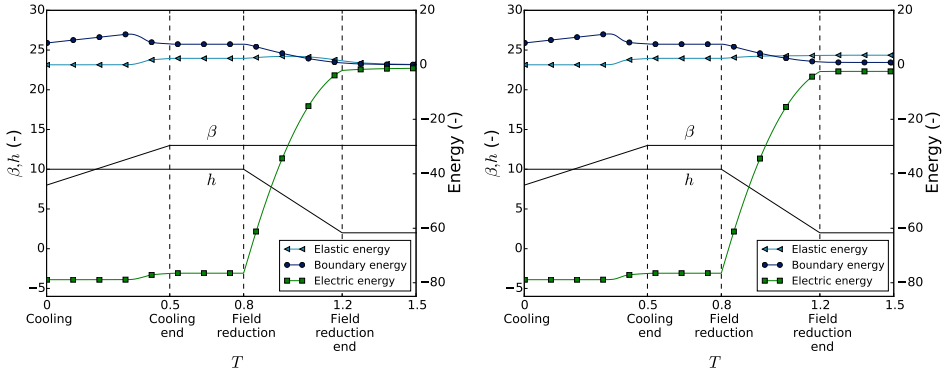

FIGURE 9. Evolution of the different terms in the discrete energy (22) as a function of time for two different realizations of the initial data.

in a basic cooling experiment. The existence of such states has recently been shown experimentally [7] and theoretically in the stationary case [2]. However, to the best of the authors' knowledge, this is the first dynamic study of how excited (odd parity) director states manifest in the weak Fréedericksz transition.

Moreover, the sensitivity of the time evolution of the weak Fréedericksz transition with regard to common modeling assumptions has been investigated. Herein, the one-constant approximation was shown to impact the dynamics of the problem when using elastic constants comparable to those of the liquid crystal 5CB. Also, to some extent, the problem was sensitive to the assumption of a constant electric field. However, substantial deviations when coupling with Maxwell's equations could only be observed for very high values of $\varepsilon_a/\varepsilon_\perp$.

ACKNOWLEDGEMENTS

The work of Peder Aursand and Johanna Ridder has been funded by the Research Council of Norway (project numbers 213638 and 214495, respectively).

REFERENCES

[1] P Aursand and U. Koley. Local discontinuous Galerkin methods for a nonlinear variational wave equation modeling liquid crystals. *Preprint*, 2014.

[2] G. Bevilacqua and G. Napoli. Parity of the weak fréedericksz transition. *Eur. Phys. J. E*, 35(12):1–5, 2012.

[3] G. P. Bryan-Brown, E. L. Wood, and I. C. Sage. Weak surface anchoring of liquid crystals. *Nature*, 399(6734):338–340, 1999.

[4] F. P. da Costa, M. Grinfeld, N. J. Mottram, and J. T. Pinto. Uniqueness in the freedericksz transition with weak anchoring. *J. Diff. Eq.*, 246(7):2590–2600, 2009.

[5] P. G. De Gennes and J. Prost. *The Physics of Liquld Crystals*. Clarendon Press, Oxford, 1993.

[6] X. Gang, S. Chang-Qing, and L. Lei. Perturbed solutions in nematic liquid crystals under time-dependent shear. *Phys. Rev. A*, 36(1):277–284, 1987.

[7] T. A. Kumar, P. Sathyanarayana, V. S. S. Sastry, H. Takezoe, N. V. Madhusudana, and S. Dhara. Temperature-and electric-field-induced inverse freedericksz transition in a nematogen with weak surface anchoring. *Phys. Rev. E*, 82(1):011701, 2010.

[8] G. R. Luckhurst, D. A. Dunmur, and A. Fukuda. *Physical properties of liquid crystals: nematics*. IET, 2001.
[9] G. Napoli. Weak anchoring effects in electrically driven freedericksz transitions. *J. Phys. A Math. Gen.*, 39(1):11, 2006.
[10] J. Nehring, A. R. Kmetz, and T. J. Scheffer. Analysis of weak-boundary-coupling effects in liquid-crystal displays. *J. Appl. Phys.*, 47(3):850–857, 2008.
[11] A Rapini and M Papoular. Distorsion d'une lamelle nématique sous champ magnétique conditions d'ancrage aux parois. *J. Phys. Colloq.*, 30(C4):C4–54, 1969.
[12] I. W. Stewart. *The static and dynamic continuum theory of liquid crystals: a mathematical introduction*. CRC Press, 2004.
[13] E. G. Virga. *Variational theories for liquid crystals*, volume 8. CRC Press, 1994.

(Peder Aursand)
Department of Mathematical Sciences,
Norwegian University of Science and Technology,
NO–7491 Trondheim, Norway.
E-mail address: peder.aursand@math.ntnu.no

(Gaetano Napoli)
Dipartimento di Ingegneria dell´Innovazione,
Università del Salento,
via per Monteroni, 73100 Lecce, Italy
E-mail address: gaetano.napoli@unisalento.it

(Johanna Ridder)
Department of Mathematics,
University of Oslo,
P.O.Box NO-1053, Blindern, Oslo-0316, Norway.
E-mail address: johanrid@math.uio.no